Large-Eddy Simulations of Tropical Convective Systems, the Boundary Layer, and Upper Ocean Coupling

Eric D. Skyllingstad
College of Oceanic and Atmospheric Sciences, Oregon State University
104 COAS Admin. Bldg.
Corvallis, OR 97331
Phone: (541) 737-5697 Fax: (541) 737-2540 Email: skylling@coas.oregonstate.edu

Simon de Szoeke
College of Oceanic and Atmospheric Sciences, Oregon State University
104 COAS Admin. Bldg.
Corvallis, OR 97331
Phone: (541) 737-8391 Fax: (541) 737-2064 Email: sdeszoek@coas.oregonstate.edu

Award Number: N00014-10-1-0299

LONG-TERM GOAL

Improve operational numerical weather prediction (NWP) models to more accurately simulate the interaction of tropical deep convection and atmospheric and oceanic boundary layers.

OBJECTIVES

Investigate tropical convection and upper ocean circulations on scales from 100 m to 200 km. Elucidate specifically how the ocean mixed layer responds to forcing from atmospheric convection such as wind and precipitation, and thus how surface fluxes depend on the history of convective events. Perform high-resolution coupled atmosphere-ocean numerical model simulations, whose fidelity is a benchmark for operational models and parameterizations. Insights gained from these simulations will be used to improve parameterizations used in operational scale models, and to refine hypotheses in collaboration with investigators working on observational field studies in the Indian and West Pacific Oceans.

APPROACH

Intraseasonal variability in the tropics is dominated by the Madden-Julian Oscillation (MJO), which generates large-scale variability in the structure and organization of deep convective cloud systems. MJO events consist of multiple scales of convective activity, from single kilometer-sized cells to circulations encompassing half of the tropical Pacific. Key factors for tropical convection include sea-surface evaporation and large-scale atmospheric moisture convergence, which both depend on sea-surface temperature and wind speed. Most numerical models do not resolve turbulent and convective scales, nor do they simulate the MJO accurately. We investigate how convection during the active phase of MJO affects and interacts with the ocean mixed layer. We conduct large eddy simulation (LES) of organized convective systems, which resolve boundary layer eddy scales to mesoscale

Report Documentation Page

Form Approved
OMB No. 0704-0188

1. REPORT DATE	2. REPORT TYPE	3. DATES COVERED
30 SEP 2014		**00-00-2014 to 00-00-2014**

4. TITLE AND SUBTITLE	5a. CONTRACT NUMBER
Large-Eddy Simulations of Tropical Convective Systems, the Boundary Layer, and Upper Ocean Coupling	5b. GRANT NUMBER
	5c. PROGRAM ELEMENT NUMBER
6. AUTHOR(S)	5d. PROJECT NUMBER
	5e. TASK NUMBER
	5f. WORK UNIT NUMBER
7. PERFORMING ORGANIZATION NAME(S) AND ADDRESS(ES) **Oregon State University,College of Oceanic and Atmospheric Sciences,104 COAS Admin. Bldg,Corvallis,OR,97331**	8. PERFORMING ORGANIZATION REPORT NUMBER
9. SPONSORING/MONITORING AGENCY NAME(S) AND ADDRESS(ES)	10. SPONSOR/MONITOR'S ACRONYM(S)
	11. SPONSOR/MONITOR'S REPORT NUMBER(S)

12. DISTRIBUTION/AVAILABILITY STATEMENT
Approved for public release; distribution unlimited

13. SUPPLEMENTARY NOTES

14. ABSTRACT

15. SUBJECT TERMS

16. SECURITY CLASSIFICATION OF:			17. LIMITATION OF ABSTRACT	18. NUMBER OF PAGES	19a. NAME OF RESPONSIBLE PERSON
a. REPORT **unclassified**	b. ABSTRACT **unclassified**	c. THIS PAGE **unclassified**	**Same as Report (SAR)**	**8**	

convective towers. These numerical simulations reveal how atmospheric convection alters air-sea fluxes and the ocean boundary layer, and will help refine hypotheses on coupling between the ocean and atmospheric boundary layer during MJO events. Processes on these scales are gaining importance in operational NWP models as the realism of convection increases along with model resolution.

WORK COMPLETED

Research during the final year of this project has focused on analyzing results from the LES to elucidate characteristics of convection during different stages of the MJO. Results presented here are taken from a publication that is currently in review (Skyllingstad and de Szoeke 2014). Work has also continued on understanding how convective systems propagate in the tropics and what relationship exists between cold pool systems and upper level winds in determining propagation speeds. A second paper is in preparation and will be submitted in the near future.

RESULTS

Previous cloud resolving model-observation comparisons have shown the importance of moisture sources in setting the strength of convection and average precipitation rates. Consistent rainfall amounts are predicted even though average model temperature and moisture content can drift significantly from observed profiles, for example as simulated by Woolnough et al. 2010 and Wang et al. 2013. Here we examine how convection responds to three different amounts of large-scale moisture convergence (Cases M100, M200 and M300) that are representative of the transition from suppressed stage to active stage of the MJO.

a) Surface wind speed

Convection in each of the cases changes in frequency, strength and overall behavior depending on the strength of moisture convergence. We plot the surface zonal wind component, u, using a time-longitude Hovmöller diagram along a line of latitude (Fig. 1), thereby representing both the eastward propagation of convective systems and their relative strength. This representation shows the acceleration of the surface wind by cold pools, which typically appears as a couplet of positive and negative velocity as a cold pool intersects the meridional location plotted. Zonal wind maxima indicate the leading edge of cold pool systems from recently active convective cells. In case M100, cold pools are generated by large, slow moving systems that last ~ 6 hours and occasionally generate a strong eastward wind gust, for example on day 7 near x = 480 km (Fig. 1a). The number of cold pool systems is limited, with relatively few interactions between cold pool edges leading to new convective cells. Cold pool edge propagation in the zonal direction is sometimes ~5 m s^{-1}, but does not show a well organized structure over time.

Case M200 produces more convective cells that tend to propagate eastward with slightly more long-lived eastward gust fronts and zonally limited westward gusts as indicated by the small regions of negative velocity that weaken and in the mean eastward wind. Gust fronts are typically active for about 100-150 km with propagation speeds between 5-8 m s^{-1}. Intersections between cold pools from different convective cells occasionally generate new convection, for example as shown by the gust front intersection just after day 7 near x = 380 km. Animations of surface temperature and specific humidity suggest that many new cells are generated along old cold pool boundaries that have well-defined temperature and humidity gradients, but do not have significant wind variations.

Cell propagation in case M450 has stronger outflows in both positive and negative directions. Systems in this case are more vigorous, long-lived, and tend to recirculate through the domain multiple times. Intersections between eastward and westward moving cold pools tend to break the symmetry of propagation, causing new cells to form that are slightly displaced in time from the original cold pool boundaries, for example on day 7 at x = 240 km. Phase speeds again range between 5-8 m s^{-1}, depending on the particular cell. As the simulation progresses, gust front systems tend to decrease in duration and propagation speed. The mean wind speed in M450 and M200 is ~3.5 m s^{-1} and ~1.5 m s^{-1} for case M100, indicating that increased convection with stronger moisture convergence increases downward vertical momentum transport from the upper level winds.

b) Vertical temperature profiles

Increasing moisture convergence also has a significant effect on the atmospheric structure, demonstrated by the average vertical temperature and dew point temperature at the end of the simulation (Fig. 2). In all of the simulations, the initial 1-2 days (during the low resolution spin up) are characterized by average cooling of the atmosphere from a net radiative flux to space. Convection typically requires 3-4 days to develop and balance this heat loss. After 9 days the moisture convergence has affected the thermal structure with larger moisture flux generating a warmer profile through greater latent heat release. Resulting temperature profiles all follow essentially moist adiabats in the upper troposphere, but display steeper lapse rates below the melting layer at ~600 hPa. To a smaller degree, observations also show an increased lapse rate at this level (Mapes 2001).

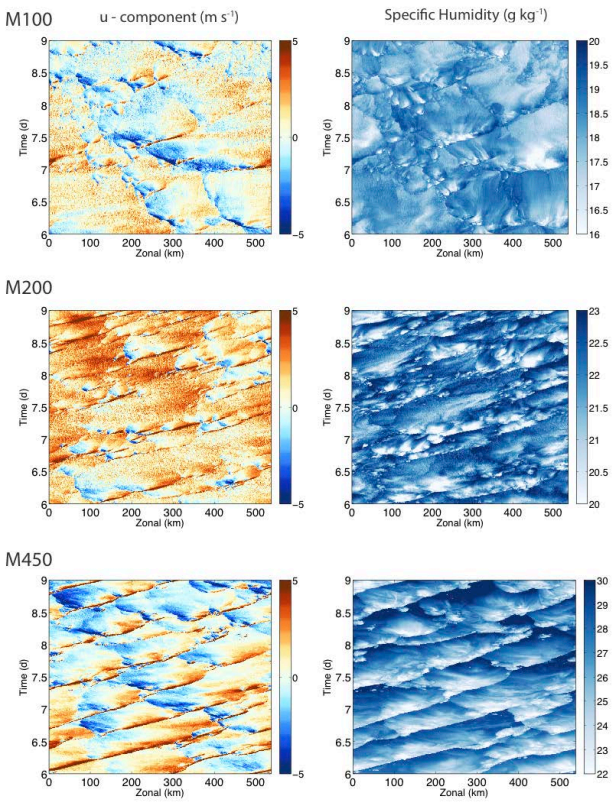

Figure 1. Hovmöller diagrams of zonal velocity and specific humidity at y = 268.8 km.

In all cases the stratosphere warms, tending to lower the height of the tropopause. This is most likely because of shortwave radiative heating that is too strong (we use the default RRTM ozone concentration profile). Greater convective mixing deepens the tropopause for cases with stronger moisture flux convergence. Case M100 shows that moisture convergence of 100 W m^{-2} is insufficient for balancing the long wave radiative cooling, leading to a new equilibrium profile with tropospheric temperatures about 4 degrees cooler than the original temperature profile. This case represents conditions during the suppressed phase of the MJO when we expect significant subsidence and tropospheric warming from the large-scale circulation, which would offset the effects of longwave radiative cooling. We also note that the simulated dew point in the upper troposphere is systematically higher than the observations. Specific humidity at these temperatures are very small, such that this error amounts to only ~0.002 g kg^{-1}.

Increasing the prescribed moisture convergence to 200 W m^{-2} (Case M200) produces a temperature sounding almost identical to the initial state between ~600 hPa and ~150 hPa indicating that for this case increased latent heat flux in the upper troposphere is appropriate for balancing long wave radiative cooling. Case M450 has a further increase in temperature and moisture where the entire troposphere temperature profiles exceeds the observed conditions by more than 5 ^{o}C. Temperatures in M200 below 600 hPa are noticeably warmer and indicate higher moisture than the baseline DYNAMO averages, but are for the most part within the spread of observed radiosonde data. Cases M200 and M450 represent the active phase of the MJO and would be expected to have an average positive velocity component with adiabatic cooling to compensate the large-scale stratiform heating profile. Mean upward motion, as diagnosed from TOGA-COARE and DYNAMO during active convective periods, would tend to both cool the sounding directly through adiabatic ascent and promote enhanced convection and vertical transport of low level moisture.

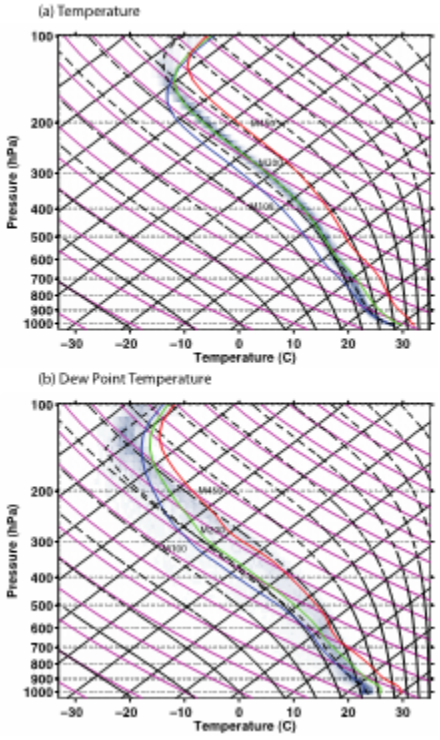

Figure 2. Horizontally averaged (a) temperature and (b) dew point temperature from the initial condition (black dashed) and at hour 216 from Case M100(blue), M200 (green) and M450 (red). Also shown are the histograms of DYNAMO radiosonde measurements (shaded).

The similarity between the M200 soundings and the observed profiles is reassuring given that the total moisture source (evaporation plus moisture convergence) in this case represents a rainfall rate consistent with the average DYNAMO rainfall (~9 mm d^{-1}) (Johnson and Ciesielski 2013). This probably represents the phase of the MJO when large-scale moisture flux is increasing, but large-scale vertical motion is small and not affecting the temperature. If we view the MJO as a single cycle of a mode 1 baroclinic wave system, for example as considered in Kuang (2008), then this would represent a nodal point where the wave-forced vertical velocity is near zero and the average temperature profile is controlled mostly by local convective processes.

c) Average heat budget

Temperature profiles can be analyzed using the vertical heat budget, defined by

$$\frac{d\bar{\theta}(z)}{dt} = -\frac{\partial\left(\overline{w'\theta'}\right)}{\partial z} + \overline{SW}(z) + \overline{LW}(z) + \overline{LH}(z)$$

where $\frac{d\bar{\theta}(z)}{dt}$ is the storage, $\frac{\partial\left(\overline{w'\theta'}\right)}{\partial z}$ is the convective vertical eddy heat flux transport, *SW* is the short wave heating, *LW* is the long wave heating, and *LH* is the net latent heat release and the over bar denotes a horizontal domain- and time-average. Plots of each term are presented in Fig. 3 for each of the moisture flux cases. Also shown is the latent heat of fusion release from transitions between frozen and liquid precipitation types. In general, each moisture convergence scenario yields heating profiles that exhibit similar vertical structures, with increasing moisture convergence leading to progressively stronger and deeper convective systems.

The overall heat budget is dominated by net radiative cooling and latent heat release concentrated below 10 km. Above 10 km, vertical transport acts to move heat released in the lower troposphere to the tropopause at 12-14 km height, and downward into the boundary layer below 1 km. Vertical eddy transport in the upper troposphere is thought to have a key role in the formation of stratiform anvil regions that define the mesoscale cloud mass in tropical clusters (Houze 2004; Mapes 2001; Houze 1997). Mid levels have very small heating from vertical transport suggesting that active updrafts are compensated by subsidence in between convective cells. As *M* increases, *LW* radiation partially offsets greater *LH* near 7-10 km and 13-15 km height, indicating a slight negative feedback that reduces warming of the profile.

Details in the latent heating profile are suggestive of various processes, for example, minimum values just below the freezing level at 5 km indicate the melting of frozen precipitation and a maximum at the boundary layer top near 1 km indicating the formation of trade wind cumulus. Cooling below the lifted condensation level is produced by the evaporation of rain unbalanced by condensation, augmenting the formation of cold pools. Splitting of the convective transport term between upward and downward motions (not shown) indicates that boundary layer cooling by evaporation is balanced by adiabatic warming during descent of air parcels having higher θ and the lifting of low θ boundary layer air under developing convective systems.

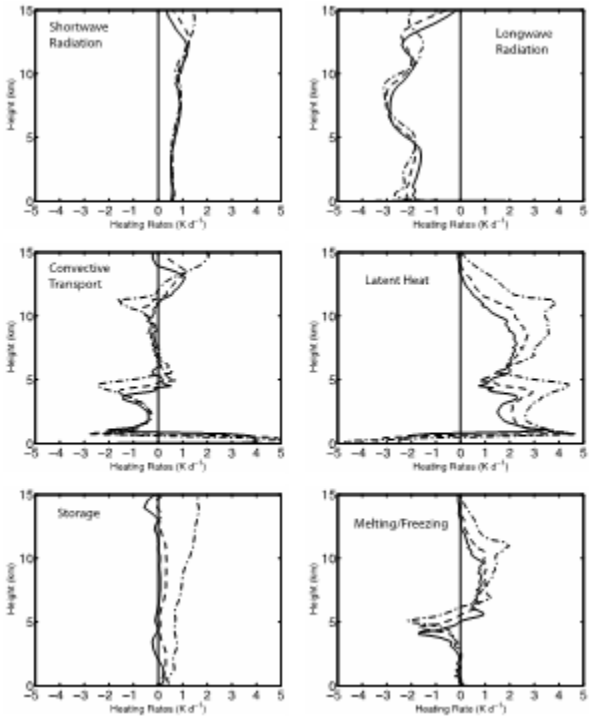

Figure 3. Heating rates averaged horizontally and over hours 144-216 for case M100 (solid), M200 (dashed) and M450 (dash-dot).

The latent heating profile in each case has three distinct maxima that can be interpreted as the trimodal tropical cloud structure described by Johnson et al. (1999). The low level peak represents boundary layer clouds, the midlevel maximum represents warm cumulus congestus, and the broad upper level maximum signifies deep convection. Key to this structure is the maximum in net latent heating around 4 km height, which may also be responsible for the reduced lapse rate just below the modeled freezing level. Lapse rate anomalies at these heights are a distinct feature of the tropical atmosphere and are thought to result from melting of precipitation (Mapes 2001; Folkins 2013) and the large-scale circulation generated by the vertical latent heat distribution associated with synoptic scale convective organization (Posselt et al. 2008). Reduced net latent heating in our simulation below the freezing level results primarily from melting of snow and graupel as demonstrated by the negative latent heating term from freezing and melting.

d) Surface flux

Changing the strength of convection through moisture convergence does not simply increase fluxes (Fig. 4). Except for the increased shear case (M100sh), changes in average specific humidity and temperature decrease latent and sensible flux as moisture convergence increases. Wind speed increases latent heat flux in case M100sh by about 40%. Fluxes for the M100sh case are consistent with DYNAMO measurements during the suppressed phase of the MJO, with sensible heat flux values much smaller than latent heat flux.

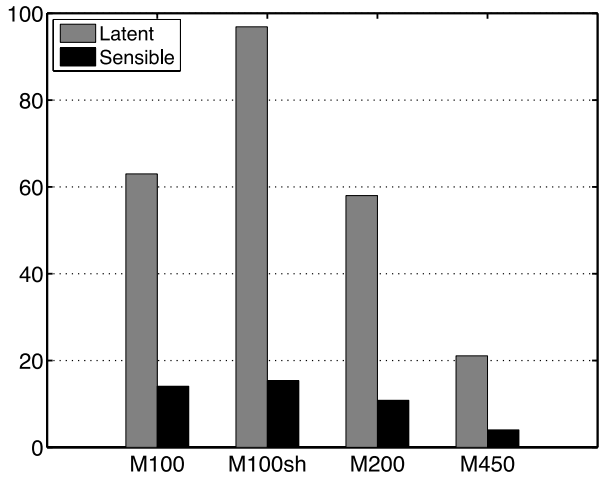

Figure 4. Latent and sensible heat flux (W m^{-2}) for each case.

Similar fluxes in case M100 and M200 and the reduction in flux in case M450 seem to imply that cloud-scale wind variations from increased convective activity does not have a significant effect on the average fluxes. Previous modeling and observational studies have shown that convection enhances surface fluxes through the action of increased winds from cold pool systems and squall lines. Our results suggest that, while convection has a role in setting surface fluxes as indicated by the enhancement of latent heat flux, changing convective intensity does not always translate into stronger surface fluxes.

RELATED PROJECTS

This project is part of the Indian Ocean Air-Sea DRI and is a part of DYNAMO. A related DYNAMO National Science Foundation project entitled "DYNAmics of the Madden-Julian Oscillation / Analysis of subsurface fluxes with coupled large-eddy simulation models" will provide a significant ocean component not proposed in the current project.

REFERENCES

Folkins, I., 2013: The melting level stability anomaly in the tropics. *Atmos. Chem. Phys*., **13**, 1167-1176.

Houze, R. A., 1997: Stratiform precipitation in regions of convection: a meteorological paradox? *Bull. Am. Meteorol. Soc*., **78**, 2179-2196.

Houze, R. A., 2004: Mesoscale convective systems. *Rev. Geophys*., **42**, doi:10.1029/2004RG000150.

Johnson, R. H., T. M. Rickenbach, S. A. Rutledge, P. E. Ciesielski, and W. H. Schubert, 1999: Trimodal characteristics of tropical convection. *J. Climate*, **12**, 2397-2418.

Johnson, R. H., and P. E. Ciesielski, 2013: Structure and Properties of Madden–Julian Oscillations Deduced from DYNAMO Sounding Arrays. *J. Atmos. Sci.*, **70**, 3157–3179.

Kuang, Z., 2008: Modeling the interaction between cumulus convection and linear internal gravity waves using a limited-domain cloud system-resolving model. *J. Atmos. Sci.,* **65**, 576-591.

Mapes, B. E., 2001: Water's two height scales: The moist adiabat and the radiative troposphere. *Q. J. R. Meteorol. Soc*., **127**, 2353-2366.

Posselt, D. J., S. C. van den Heever, and G. L. Stephens, 2008: Trimodal cloudiness and tropical stable layers in simulations of radiative convective equilibrium. *Geophys. Res. Lett.,* **35**, doi:10.1029/2007GL033029.

Wang, S., A. H. Sobel, and Z. Kuang, 2013: Cloud-resolving simulation of TOGA-COARE using parameterized large-scale dynamics. *J. Geophys. Res*., **118**, 6290-6301.

Woolnough, S. J., P. N. Blossey, K.-M. Xu, P. Bechtold, J.-P. Chaboureau, T. Hosomi, S. F. Iacobellis, Y. Luo, J. C. Petch, R. Y. Wong, and S. Xie, 2010: Modelling convective processes during the suppressed phase of a Madden-Julian oscillation: Comparing single-column models with cloud-resolving models. *Q. J. R. Meteorol. Soc*., **136**, 333-353.

PUBLICATIONS

Skyllingstad, E. D., and S. P. de Szoeke, 2014: Cloud-resolving large-eddy simulation of tropical convective development and surface fluxes. *Mon. Wea. Rev.,* submitted.